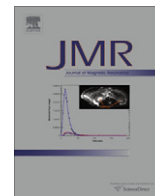


Contents lists available at [SciVerse ScienceDirect](http://www.sciencedirect.com)

Journal of Magnetic Resonance

journal homepage: www.elsevier.com/locate/jmr

Magnetic resonance of calcified tissues

Felix W. Wehrli*

Laboratory for Structural NMR Imaging, Department of Radiology, Perelman School of Medicine, University of Pennsylvania, United States

ARTICLE INFO

Article history:

Received 15 November 2012

Revised 13 December 2012

Available online xxxxx

Keywords:

Calcified tissues

Bone

Structure

Function

Biomechanics

Ultra-short echo-time

Porosity

Collagen

Deuterium NMR

31P MRI

Magnetic susceptibility

Diffusion

 T_2^*

ABSTRACT

MRI of the human body is largely made possible by the favorable relaxation properties of protons of water and triacyl glycerides prevalent in soft tissues. Hard tissues – key among them bone – are generally less amenable to measurement with in vivo MR imaging techniques, not so much as a result of the lower proton density but rather due to the extremely short life-times of the proton signal in water bound to solid-like entities, typically collagen, or being trapped in micro-pores. Either mechanism can enhance T2 relaxation by up to three orders of magnitude relative to their soft-tissue counterparts. Detection of these protons requires solid-state techniques that have emerged in recent years and that promise to add a new dimension to the study of hard tissues. Alternative approaches to probe calcified tissues exploit their characteristic magnetic properties. Bone, teeth and extra-osseous calcium-containing biomaterials are unique in that they are more diamagnetic than all other tissues and thus yield information indirectly by virtue of the induced magnetic fields present in their vicinity. Progress has also been made in methods allowing very high-resolution structural imaging of trabecular and cortical bone relying on detection of the surrounding soft-tissues. This brief review, much of it drawn from work conducted in the author's laboratory, seeks to highlight opportunities with focus on early-stage developments for image-based assessment of structure, function, physiology and mechanics of calcified tissues in humans via liquid and solid-state approaches, including proton, deuterium and phosphorus NMR and MRI.

© 2013 Elsevier Inc. All rights reserved.

1. Chemistry, architecture and physiology of bone

Bone is a hierarchically organized biomaterial evolved so as to optimally fulfill its multiple functions ranging from weight-bearing and locomotion to serving as a store for calcium and phosphorus. The major chemical constituents of bone are an organic fraction, consisting predominantly of type-I collagen (~50% by volume), an inorganic or mineral fraction (~35%), made up of poorly mineralized nonstoichiometric calcium hydroxyl apatite with a much smaller and variable fraction of carbonate apatite. The balance is water, with its majority bound to collagen, and a smaller fraction occupying the bone's pore structure. The mineral crystals are interspersed in the gaps between successive collagen fibrils [1]. The bone's compressive strength is largely conferred by the material's inorganic component whereas collagen is responsible for the bone's tensile strength. On a macrostructural level bone is about 80% compact (or cortical) and 20% trabecular. Cortical bone forms the shell encasing bone marrow and blood vessels, dominating the shaft of the extremities and femoral neck whereas trabecular bone, consisting of a meshwork on interconnected plates and rods, is dominant in the vertebrae, ribs and near the joints where stresses are multidirectional and tensile and torsional loading occurs.

Bone is a living tissue with its own blood supply and ability for self-repair through a process called 'remodeling', referring to the interplay of two types of cells: osteoblasts, the bone-forming, and osteoclasts, the bone-resorbing cells. A third type of cells, the osteocytes occupying small cavities on the order of 30 μm in diameter, act as pressure transducers providing signals to osteoblast to induce bone formation. Osteocytes are interconnected with each other through a system of channels, called canaliculi, about 100 nm in diameter. Cortical bone further is permeated by a network of channels, on the order of 50–100 μm in diameter, carrying blood vessels, in contrast to the blood supply to trabecular bone, which is effected through the marrow's microvascular system.

2. Indirect detection of trabecular and cortical bone microstructure

We refer to 'indirect detection' of microarchitecture methods that obviate the need for resolving individual trabecular elements (which are on the order of 100 μm thickness) in trabecular bone or, for example, pore volume fraction in cortical bone (with pore diameters ranging from 10 to several hundred micrometers), thereby obviating the need to resolve individual structural elements. Such approaches entail significant advantages in terms of signal-to-noise (SNR) requirements.

* Fax: +1 215 662 7263.

E-mail address: wehrli@mail.med.upenn.edu

3. Methods exploiting internal magnetic fields for the study of trabecular bone architecture

3.1. Static dephasing regime

The majority of low-resolution MRI studies of bone architecture exploit the bone's diamagnetic properties. The greater density of higher atomic-number elements in bone mineral (notably calcium and phosphorus) render bone tissue considerably more diamagnetic than bone marrow (by about 3 ppm, S.I.) [2]. Compartmentalization of the two phases (i.e. bone and marrow) leads to induced inhomogeneous magnetic fields near the interface of the two phases [3].

The empirical observation of a rapid decay of the trabecular bone marrow FID or gradient echo thus results from local induced field gradients (also referred to 'internal magnetic field gradients' IMFG). The signal $S(t)$ in the presence of a mesoscopic perturber such as a trabecula in a small volume element as, for example, an imaging voxel can be written as

$$S(t) = \iiint_V M_{\perp}(0) \exp(i\gamma \Delta H_z(x, y, z) \cdot t) dx dy dz \quad (1)$$

where $\Delta H_z(x, y, z)$ represents the local induced field, i.e. the offset from the nominal field.

Based on a magnetic surface-charge model, Hwang and Wehrli [4], computed the induced magnetic field from 3D trabecular bone images and showed the local field to result in a distribution whose mean and variance depend on the orientation of the static magnetic field relative to the structure. These findings are, of course, a consequence of the structural anisotropy of trabecular bone, which is known to grow and remodel in response to the stresses to which is subjected (Wolff's Law). Since the induced magnetic surface charge density scales as the scalar product of the surface normal \mathbf{n} and the applied magnetic field \mathbf{H}_0 as

$$\sigma \approx \mu_0 \Delta \chi \mathbf{H}_0 \cdot \hat{\mathbf{n}} \quad (2)$$

(valid as long as for the susceptibility difference between the two materials, $|\Delta \chi| \ll 1$ holds), trabecular plates perpendicular to the applied field get magnetized preferentially. There are various approaches to compute the induced field. In [4] the authors resorted to a surface triangulation method by computing the induced field $\mathbf{H}_{\text{induced}}$ at location \mathbf{r} as the sum of the induced fields from all source locations \mathbf{r}' as

$$\mathbf{H}_{\text{induced}} = \sum_{p=1}^N \mathbf{H}_{\text{induced}, p}^{\text{triangle}} = \frac{1}{4\pi\mu_0} \sum_{p=1}^N \int_{T_p} \sigma(\mathbf{r}') \frac{(\mathbf{r} - \mathbf{r}')}{|\mathbf{r} - \mathbf{r}'|^3} dA' \quad (3)$$

where N is the number of triangles and the integral represents the induced field from a single source location. The authors showed that the computation is greatly simplified by assuming that each triangular element has constant surface-charge density given by Eq. (2). The expected structural anisotropy is evident from the histograms of the induced magnetic field computed for the three orthogonal directions of the applied magnetic field relative to the major loading axis, shown for a specimen of human trabecular bone from the vertebrae (Fig. 1). The same authors subsequently evaluated their model by field mapping [5]. From the slopes of regression between the experimental and computed fields they obtained the absolute susceptibility of bone as -11.0×10^{-6} (S.I.), which is in close agreement with a reported value of -11.3×10^{-6} obtained with powdered bone by means of a spectroscopic susceptibility matching technique referred to previously [2].

The width of the induced magnetic field distribution over the sample volume (such as an imaging voxel) can be measured, for example with an asymmetric echo technique for which the echo amplitude evolves as $\exp(-2\tau/T_2')$ where τ is the echo offset [6].

Other pulse sequences based on combining RF and gradient echoes such as GESFIDE (gradient-echo sampling of FID and echo) [7] or GESSE (gradient-echo sampling of spin echo) [8] yield both T_2 and T_2^* and thus T_2' as $1/T_2' = 1/T_2$. The full width at half maximum, ΔH , of the distribution of the induced field, $P(H_{\text{induced}})$, then is related to T_2' as $T_2' = \gamma \Delta H / 2$. Spectroscopic approaches have also been practiced to obtain T_2' from the line width of the marrow water or methylene resonance [9].

Yablonskiy and Haacke had previously developed a theory for magnetically heterogeneous materials such as trabecular bone or networks of blood vessels, showing that the concept of an exponential time constant T_2' is valid in the *static dephasing regime*, but only for decay times longer than a critical time t_c [10]. The static dephasing regime essentially implies that dephasing from local inhomogeneous fields is much faster than phase-coherence loss of magnetic moments as they visit sites of different magnetic field during diffusion, a condition that is generally satisfied for fatty bone marrow but, as we shall see, not necessarily in the cellular boundary zone lining the trabecular trabecular bone surface [11]. Yablonskiy and Haacke's model also showed R_2' ($=1/T_2'$) to scale with the volume fraction of the perturber (i.e. bone in the present case) and further that it has an angular dependence for anisotropic structures. The latter arrangement, as previously pointed out, is typical of trabecular networks, which preferentially align along the bone's major loading axis. For an array of mutually perpendicular struts and columns such similar to the trabeculae found in the vertebrae or in the radius (cf. Fig. 1), the model predicts R_2' to obey the following relationship [10]:

$$R_2' \propto \Delta \chi H_0 \left\{ \zeta_h + \left(\zeta_v - \frac{1}{2} \zeta_h \right) \sin^2 \vartheta \right\} \quad (4)$$

where ζ_h and ζ_v represent the volume fractions of struts and columns and ϑ is the angle between the magnetic field and the columns. The predictions of Eq. (4) are in good semiquantitative agreement with experimental findings in model structures [12,13], specimens of trabecular bone [14] as well as measurements in vivo in humans [15].

Measurements of T_2^* or T_2' have allowed discrimination of patients with osteoporotic bone loss and structural degradation of the trabecular bone network at various anatomic sites including the distal radius, vertebrae and hip, all common fracture sites, as well as at surrogate locations such as the calcaneus (for recent reviews of the subject, see, for example [16]). In general, regional relaxation rates were found to parallel apparent density measured by dual-energy X-ray absorptiometry or quantitative computed tomography. Some of this work has shown T_2' or T_2^* to discriminate patients with from those without fractures as well or better than bone densitometry [9,17]. However, the translational aspects of these methods are of primary interest to the clinical imaging community and are thus somewhat outside the intended scope of this article.

3.2. Diffusion in background magnetic field gradients

There has been recent evidence that the notion of the static dephasing regime, generally assumed to apply to protons in the marrow spaces exposed to the internal magnetic field gradient (IMFG) at the bone–bone–marrow boundary, may not necessarily be valid [18,19]. If the primary interest is the evaluation of the IMFG this can be achieved with a simple field map, obtained, for example from 3D high-resolution trabecular bone images, such as those reported by Hwang and Wehrli [4], yielding both magnitude and direction of the IMFG as $\nabla H_z(x, y, z)$ where $H_z(x, y, z)$ is the local induced magnetic field. Of course, such an approach would require imaging at a resolution adequate to resolve

Download English Version:

<https://daneshyari.com/en/article/5405721>

Download Persian Version:

<https://daneshyari.com/article/5405721>

[Daneshyari.com](https://daneshyari.com)